Resolution enhancement of optical scanning holography with a spiral modulated point spread function

Ni Chen,[1] Zhenbo Ren,[1] Haiyan Ou,[2] and Edmund Y. Lam[1,*]

[1]*Department of Electrical and Electronic Engineering, The University of Hong Kong, Pokfulam, Hong Kong, China*
[2]*Institute of Applied Physics, University of Electronic Science and Technology of China, 610054 Chengdu, China*
**Corresponding author: elam@eee.hku.hk*

Received August 26, 2015; revised November 2, 2015; accepted November 4, 2015;
posted November 10, 2015 (Doc. ID 248509); published December 15, 2015

In optical scanning holography, one pupil produces a spherical wave and another produces a plane wave. They interfere with each other and result in a fringe pattern for scanning a three-dimensional object. The resolution of the hologram reconstruction is affected by the point spread function (PSF) of the optical system. In this paper, we modulate the PSF by a spiral phase plate, which significantly enhances the lateral and depth resolution. We explain the theory for such resolution enhancement and show simulation results to verify the efficacy of the approach.

OCIS codes: (090.1995) Digital holography; (110.1758) Computational imaging; (110.4850) Optical transfer functions.
http://dx.doi.org/10.1364/PRJ.4.000001

1. INTRODUCTION

Optical scanning holography (OSH) is a digital holographic technique that records the volumetric information of a three-dimensional (3D) scene by two-dimensional (2D) scanning [1]. Compared with other forms of digital holography, OSH has distinct advantages, such as fluorescence imaging [1,2] and partially coherent illumination [3]. In addition to developing OSH applications, such as microscopy and remote sensing, compressive sensing [4], sectional reconstructions [5], and others [6], much attention has been focused on improving the resolution of the OSH system [7]. Several different techniques have been developed for this purpose. It has been shown that image resolution can be enhanced by obtaining more information about the object, such as the multiple detection techniques with synthetic apertures [8], dual wavelengths (DW-OSH) [9], double detection [10], and using configurable pupils (CP-OSH) [11]. Meanwhile, another approach is to manipulate the point spread function (PSF) of the OSH system by designing the pupils [12–14]. In this way, the system does not need extra time to record more information about the object, thus making it more suitable in applications where the capture time is more constrained.

In this paper, we propose a new way to enhance the resolution of the OSH reconstruction by designing the PSF with a spiral phase plate (SPP), an approach we call SPP-OSH. The SPP has been applied to other applications due to its capability in edge enhancement [15–17]. Recently, it also has been applied to the OSH [18,19], where the SPP is used to modulate one of the two beams to achieve edge enhancement or resolution enhancement. For the former, the open aperture in the conventional OSH is replaced by an SPP, such that the scanning pattern is the interference of a plane wave beam and a vortex beam. In this work, however, the SPP is used as a modulation to the spherical wave arising from one of the pupils, such that the interference at the scanning plane is from a spherical wave beam and a vortex. This produces a denser PSF, improving both the lateral and depth resolutions while enhancing the edges. The theory is explained in Section 2 and verified by simulation in Sections 3 and 4.

2. PRINCIPLE OF THE SPP-OSH SYSTEM

The proposed SPP-OSH system is shown in Fig. 1. Similar to the conventional OSH system, the laser light source with a frequency ω is divided into two paths with a beam splitter. One path goes through a pupil p_1 and a thin lens L_1 to form a spherical beam. For the other path, which passes through an acousto-optic frequency shifter (AOFS), a $4f$ system is placed instead of a single pinhole pupil p_0 in the conventional OSH, as the part in the blue-dashed rectangle enclosed in Fig. 1 shows. Thin lens L_2 and L_3 with focal length f form the $4f$ system. An SPP and the pupil p_0 are placed at the front focal plane of L_2, while the pupil p_2 is located at its back focal plane of L_2. Thus, the output from this path is a time-varying vortex beam. Unlike in the conventional OSH, where the scanning pattern is the interference between a spherical beam and a plane wave, in SPP-OSH, the plane wave is replaced by a vortex beam. The pattern is reflected by a scanning mirror into a 3D object located at a distance z. The transmitted optical wave passing through the 3D object becomes an electrical signal on the photodetector, which is turned into a digital hologram. Because the pattern used to scan the object is the interference of the two beams, the optimum location of the object is the position where the two beams have the same size. Because the size of the two beams is limited by the pupils of the objective lens, the apertures are chosen to match the later. Therefore, the same aperture size for p_0, p_1, and p_2 with radius of R is chosen. In this system, the SPP can be a digital holographic element or spatial light modulator. Furthermore, the SPP used in our system has a topological charge of 1, leading to a uniform edge enhancement for the whole object [20], with a transmittance function:

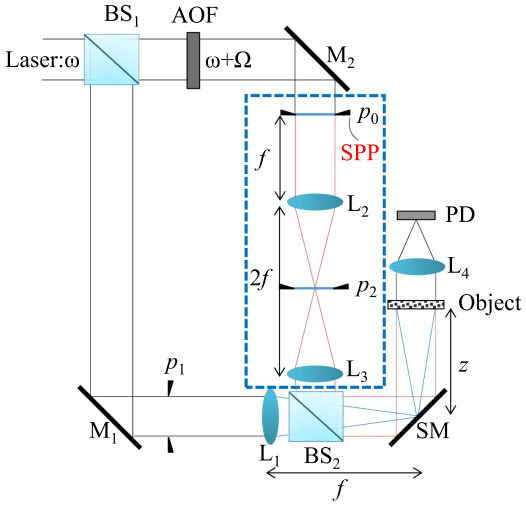

Fig. 1. Scheme of the proposed SPP-OSH system. BS_n, beam splitters; AOF, acousto-optic frequency shifter; M_n, mirror; p_n, pupils; L_n, thin lens; SM, scanning mirror; PD, photodetector.

$$t(r,\theta) = \mathrm{circ}\left(\frac{r}{R}\right)\exp(-j\theta), \tag{1}$$

where $\mathrm{circ}(r) = 1$ for $r \le 1$ or else $\mathrm{circ}(r) = 0$, R is the radius of the aperture, and (r,θ) are the polar coordinates, where $r^2 = x^2 + y^2$ and $\theta = \arctan(y/x)$. The wavefront at the back focal plane of L_2 is the Fourier transform of Eq. (1), i.e.,

$$p_2(\rho,\varphi) = \frac{k\pi R}{2f\rho}\exp\left[j\left(\varphi+\frac{\pi}{2}\right)\right][H_0(\xi)J_1(\xi) - H_1(\xi)J_0(\xi)], \tag{2}$$

where λ is the wavelength of the light source, $k = 2\pi/\lambda$ is the wavenumber, $\xi = 2\pi R\rho$ and (ρ, φ) are the polar coordinates in the spatial frequency domain, with $\rho^2 = k_x^2 + k_y^2$ and $\varphi = \arctan(k_y/k_x)$. J_n is the n-th order Bessel function, while H_n is the n-th order Struve function. p_2 can be regarded as the pinhole pupil function of the conventional OSH system. In the conventional OSH, the optical transfer function (OTF) is related to the aperture functions [14], which can be rewritten in the polar coordinate as

$$H(\rho,\varphi;z) = \exp\left[j\frac{z}{2k}\rho^2\right]\int_0^{2\pi}\int_0^{\infty} p_1^*(r')p_2(r'+r) \times \exp\left[j\frac{z}{f}r'\rho\cos(\theta-\varphi)\right]\mathrm{d}r'\mathrm{d}\theta. \tag{3}$$

In the proposed system, the wavefront at the back focal plane of L_2 is processed sequentially as the wavefront at the pinhole plane in the conventional OSH system. Substituting Eq. (2) into Eq. (3), we obtain the OTF of the proposed SPP-OSH system as

$$\begin{aligned} H(\rho,\varphi;z) &= \exp\left[j\frac{z}{2k}\rho^2\right]\int_0^{2\pi}\int_0^{\infty} p_2\left(\frac{r'+r}{R}\right) \times \exp\left[j\frac{z}{f}r'\rho\cos(\theta-\varphi)\right]\mathrm{d}r'\mathrm{d}\theta \\ &= \exp\left[-j\frac{z}{2k}\rho^2\right]\Im\{p_2^*(r,\theta)\}, \end{aligned} \tag{4}$$

where $\Im$ is the operation of Fourier transform and $\rho \le R$. The PSF of the SPP-OSH can be easily obtained by inverse Fourier transform of the OTF, i.e.,

$$\begin{aligned} h(r,\theta;z) &= \Im^{-1}\left\{\exp\left[-j\frac{z}{2k}\rho^2\right]\Im\{p_2^*(r,\theta)\}\right\} \\ &= \left\{-\frac{k}{2\pi z}\exp\left[j\frac{k}{2z}r^2\right]\right\}\left\{\pi^2 r\left(\frac{k}{2\pi z}\right)^{\frac{1}{2}} \times \exp\left[j\left(\theta-\frac{\pi}{4}\right)\right]\left[J_0\left(\frac{kr^2}{2z}\right) - jJ_1\left(\frac{kr^2}{2z}\right)\right]\right\}\mathrm{circ}\left(\frac{rf}{zR}\right), \end{aligned} \tag{5}$$

where the effect of R is ignored because the size of the apertures p_0, p_1, and p_2 are the same.

From Eq. (5), it can be observed that the PSF in the SPP-OSH system can be regarded as a combination of two terms. The first has the form of the PSF in the conventional OSH system, while the second is the spiral phase term with the Bessel functions. The quadratic phase factor of the second term has the same coefficient as the first, thus doubling the density of the fringe. The spiral phase filter performs isotropic edge enhancement because of its radial Hilbert transformation property [21]. For a diffraction-limited optical system, the maximum spatial frequency (cut-off frequency) is partially limited by the exit apertures. The higher spatial frequency components of an image are usually the edges. With this edge enhancement property of the SPP, higher spatial frequencies can be reconstructed. The analysis will be explained in the next section.

With the PSF, the hologram recording and reconstruction undergo similar processing as the conventional OSH, which can be described mathematically by

$$g(x,y;z) = \int_{-\infty}^{\infty} O(x,y;z) * h(x,y;z)\mathrm{d}z, \tag{6}$$

where $O(x,y,z)$ is the object, and $*$ is the 2D convolution. The reconstruction of an image from this hologram also can be done similarly as the conventional OSH [2].

3. RESOLUTION ANALYSIS

In the previous section, we described the proposed SPP-OSH system and the PSF, which is the combination of a conventional PSF with doubled oscillation frequency and an SPP phase term. In this section, we analyze the resulting resolution of the hologram reconstruction.

In the conventional OSH system, the lateral resolution is $\delta x = 0.61\lambda/\mathrm{NA}$ and the depth resolution is $\delta z = 2\lambda/\mathrm{NA}^2$ [22], where NA is the numerical aperture of the system. For the SPP-OSH system, the quadratic phase term in the PSF reveals that the spatial frequency is doubled; thus, within the same aperture size, the cut-off frequency of the SPP-OSH system is also doubled. Consequently, the lateral resolution of the SPP-OSH is $\delta x' = \delta x/2$. Furthermore, because the phase of the PSF changes with a distance $z/2$, the depth resolution should be $\delta z' = \delta z/2$. Putting these together, the proposed SPP-OSH has twice the resolution in both the lateral and depth directions compared with the conventional OSH.

We examine this analysis with simulations. Let the wavelength of the light source be 543 nm. Consider the finite size of the optical components, where the field of view has a radius

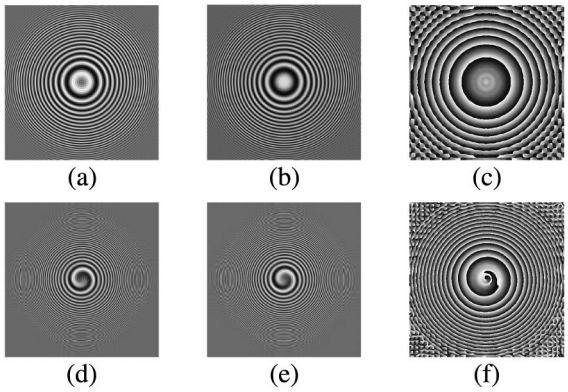

Fig. 2. (a) Real part, (b) imaginary part, and (c) phase profile of the hologram recorded with the conventional OSH; (d) real part, (e) imaginary part, and (f) phase profile of the hologram recorded with the proposed SPP-OSH.

of 0.5 mm. The focal length of the thin lens is 20 mm. A pinhole with a diameter of 1 μm located at a distance 10 mm from the scanning plane is used in this simulation. Holograms using the conventional OSH and the proposed SPP-OSH are generated, respectively. Figure 2 shows the simulation results, where (a)–(c) are the real part, imaginary part, and phase profile of the OSH hologram, and (d)–(f) are the real part, imaginary part, and phase profile of the SPP-OSH hologram, respectively. As expected, the Fresnel zone number in the SPP-OSH is doubled because of the doubled spatial frequency. However, the resolution could not be better than this ideal value considering the effects from all the apertures during the whole OSH process, as demonstrated in Ke *et al.* [9].

A. Lateral Resolution Enhancement

The lateral resolution is measured by detecting the size of the reconstructed images at the focal plane. The reconstructed images from the holograms in Fig. 2 are shown in Fig. 3, where Figs. 3(a) and 3(b) show the reconstructed images of the conventional OSH and the SPP-OSH, respectively. In Fig. 3(c), the two curves are the intensity distributions across the center horizontal lines in Figs. 3(a) and 3(b). Their full width at half-maximum (FWHM) values are approximately 11.27 μm (for conventional OSH) and 5.88 μm (for SPP-OSH), which are consistent with the theoretical values of $\delta x = 13.2$ μm and $\delta x' = 6.6$ μm.

B. Depth Resolution Enhancement

The depth resolution is measured by detecting the defocus size of the reconstructed images along the optical axis near the focal plane. Figures 4(a) and 4(b) show such images of the conventional OSH and the SPP-OSH, respectively. Similar to the above, in Fig. 4(c), the two curves are the intensity distributions across the center horizontal lines in Figs. 4(a) and 4(b). Their FWHM values are approximately 1.54 μm (for conventional OSH) and 0.86 μm (for SPP-OSH), which are also consistent with the theoretical values of $\delta z = 1.74$ μm and $\delta z' = 0.87$ μm.

C. Edge Enhancement

The PSF in Eq. (5) also contains a spiral phase term, which enhances the edges in the reconstruction. We demonstrate this with the use of a resolution chart shown in Fig. 5, which

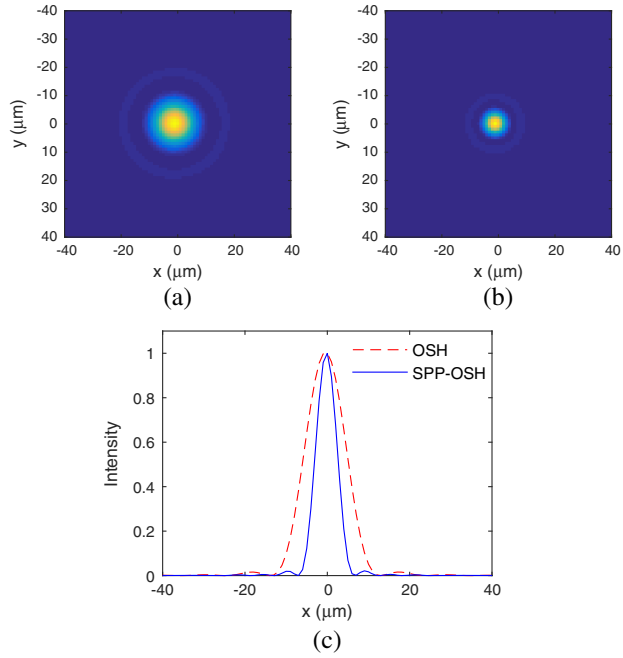

Fig. 3. Hologram reconstructions of a pinhole. Intensity profile of the reconstruction using (a) the OSH and (b) SPP-OSH. (c) Plot image across the center of the reconstructed point.

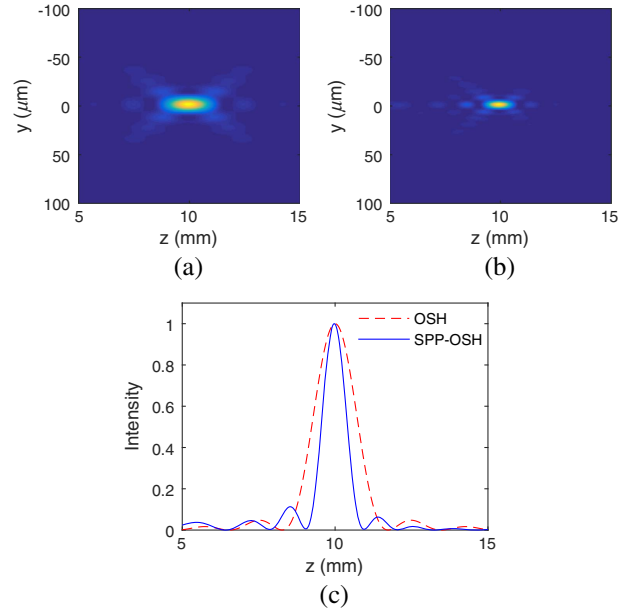

Fig. 4. Hologram reconstructions of a pinhole. Intensity profile of the reconstruction using (a) the OSH and (b) SPP-OSH. (c) Plot image across the center of the reconstructed point.

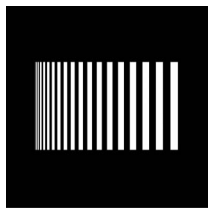

Fig. 5. Resolution chart.

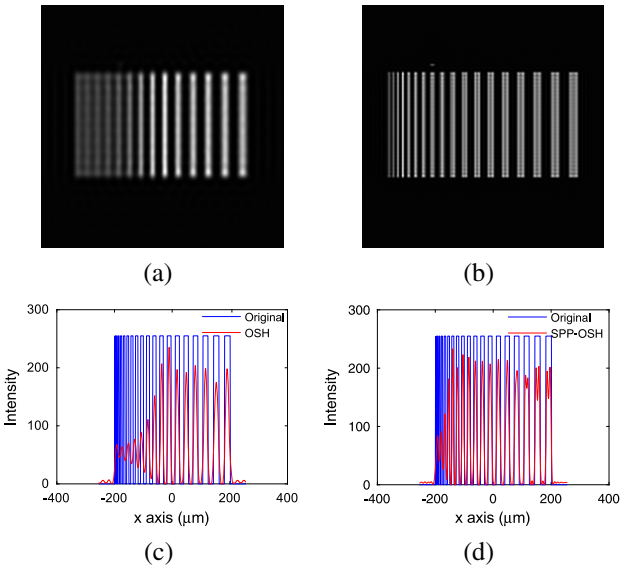

Fig. 6. Reconstructed images of the resolution chart at the focal plane of the object with (a) OSH and (b) SPP-OSH. Corresponding plot profiles across the horizontal centerlines are given in (c) and (d).

contains a group of lines with a width from 1 to 20 μm. Figures 6(a) and 6(b) show the reconstructed images with the OSH and SPP-OSH, respectively, and Figs. 6(c) and 6(d) show the plot profile along the central horizontal line. Beside the lateral resolution enhancement, SPP-OSH enhances the edges proportional to the linewidth. This is because, for the higher-resolution components, the PSFs of the OSH and the SPP-OSH perform approximately the same action. In contrast, for the lower-frequency components, the isotropic edge enhancement of the PSF of the SPP-OSH plays a major role.

Based on the above analysis, we can see that the proposed SPP-OSH system achieves lateral and depth resolution enhancement as well as enhances the edges in the images. In what follows, we use the inverse imaging approach, making use of block Jacobi-type restrictive preconditioned conjugate gradient (BJ-RPCG) [23] for the reconstruction of sectional images from the hologram.

4. NUMERICAL EXPERIMENTS

A. Lateral Resolution Verification

The same parameters and resolution chart in Section 3 are used to verify the lateral resolution enhancement. The reconstructed images and the comparison with the original image are shown in Fig. 7, where the minimum width lines are the same. However, different from Fig. 5, the SPP-OSH has no grooves for the right wider lines, suggesting that the BJ-PRPCG reconstruction has compensated the edge enhancement without affecting the resolution.

B. Depth Resolution Verification

To verify the depth resolution enhancement, 3D objects consisting of several discrete slices are used in the simulation. There is a depth difference Δz between two adjacent object slices. The discrete 3D object thus can be expressed as

$$O(x,y;z)=\sum_{n=1}^{N}O(x,y;z_n), \tag{7}$$

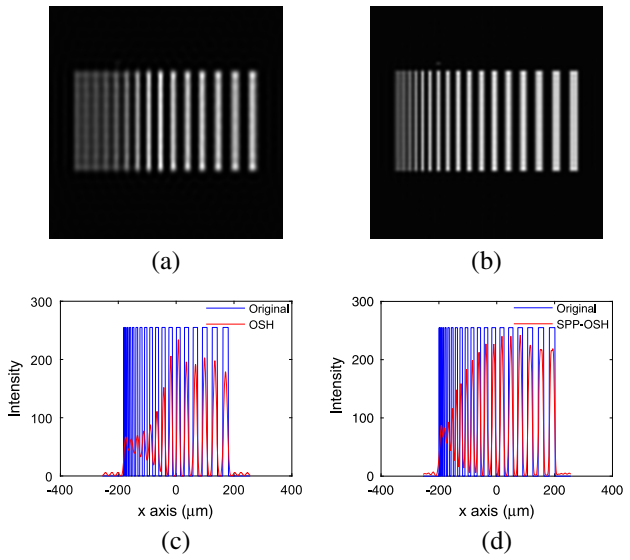

Fig. 7. Example 1: Resolution chart reconstructions with the OSH in (a) and (c); with the SPP-OSH in (b) and (d).

where N is the slice number. The hologram for this discrete 3D object becomes

$$g(x,y;z)=\sum_{n=1}^{N}O(x,y;z_n)*h(x,y;z_n). \tag{8}$$

In the following experiment, we let $N=2$. Figures 8(a) and 8(b) are the two plane images of the object used in this

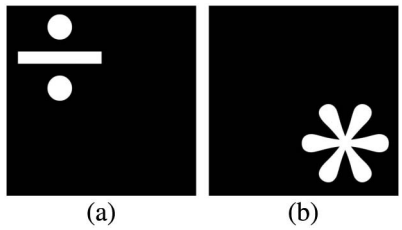

Fig. 8. Object with two plane images located at (a) z_1 and (b) z_2.

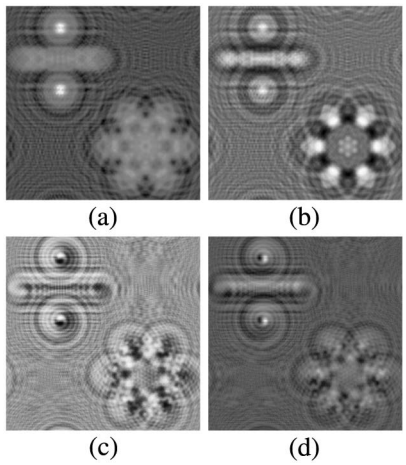

Fig. 9. (a) Real part and (b) imaginary part of the conventional OSH hologram; (c) real part and (d) imaginary part of the proposed SPP-OSH hologram.

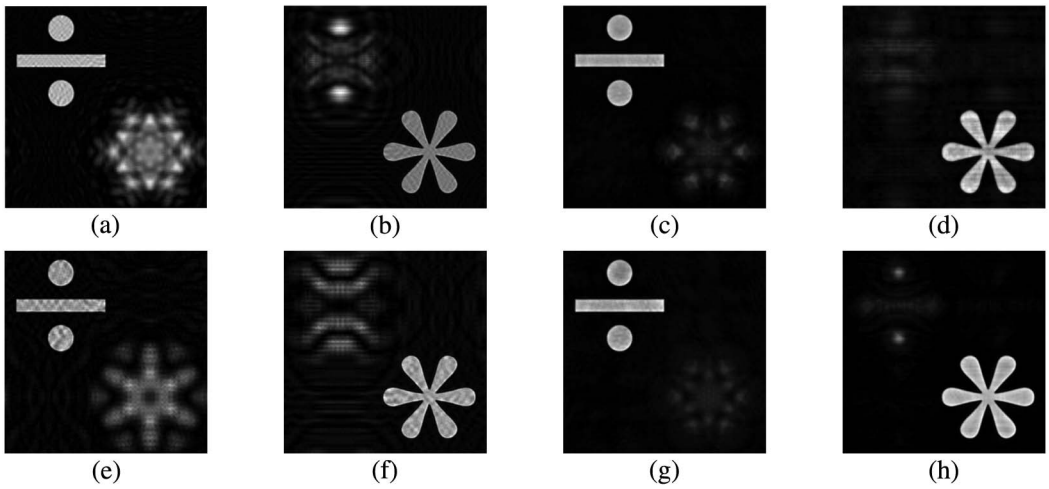

Fig. 10. Reconstructed images while $\Delta z = 5.5$ mm (first row) and 11 mm (second row), using the OSH method, given in (a), (b), (e), and (f); similar figures using the SPP-OSH method are given in (c), (d), (g), and (h).

simulation, each having a size of 512×512 pixels and representing a size of 2 mm × 2 mm. The wavelength of the illumination laser is 543 nm, and the focal length of the lens is 10 mm. Therefore, δz is approximately 11 and 5.5 mm for the OSH and SPP-OSH, respectively.

With the objects shown in Fig. 8, holograms are generated using the conventional and proposed systems, respectively, as shown in Fig. 9. Figure 10 shows the reconstructions with $\Delta z = 5.5$ mm and $\Delta z = 11$ mm, respectively. The defocus noise caused by another section is more obvious in the conventional OSH than in the SPP-OSH. Quantitatively, normalized cross correlation (NCC) is used to assess the severity of the defocus noise. We compute the correlation between the reconstructed images and the original images of a series of Δz, ranging from 1 to 20 mm, with an interval of 1 mm. The correlation coefficients of the reconstructed images versus the depth distance between the object planes are shown in Fig. 11. At different plane separations, the SPP-OSH outperforms the conventional OSH by a significant margin.

We also compare our SPP-OSH with the DW-OSH, which require two hologram detections illuminated with different wavelengths. In this simulation, one wavelength is the same as before, and the other one is 430 nm. As Fig. 12 shows, the DW-OSH can reach a better correlation very fast and become steady as Δz increases. This result can be expected from the resolution definition of $\delta z = 2\lambda/\mathrm{NA}^2$, where, for the SPP-OSH, the difference is only a factor of 2. However, in the DW-OSH, the resolution is directly related to the second wavelength. In this simulation, the second illumination wavelength of 430 nm can reach a depth resolution of $430/532 = 0.8$ times the one using a single illumination. Furthermore, the extra hologram records more information of the object. Although we apply the SPP to only one single hologram, it easily can be adapted to the dual wavelength or double detection approaches [9].

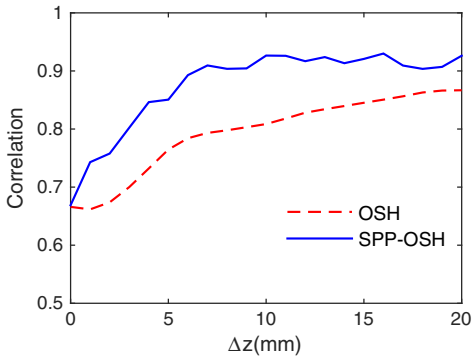

Fig. 11. Comparison of the SPP-OSH and OSH: the correlation between the reconstructed images and the original images in terms of the depth interval of the object planes.

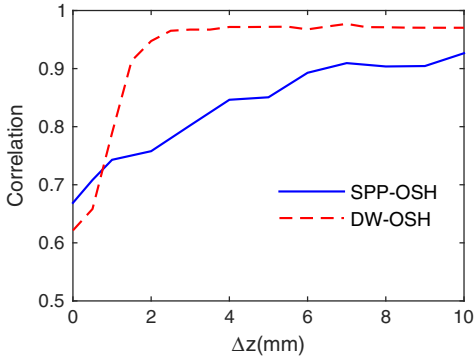

Fig. 12. Comparison of the SPP-OSH and DW-OSH: the correlation between the reconstructed images and the original images in terms of the depth interval of the object planes.

5. CONCLUSIONS

In this paper, we propose a resolution enhancement technique by using an SPP to modulate the PSF of the OSH. The theory and the numerical experiments show that the lateral and depth resolutions are doubled, compared with the conventional OSH system.

Acknowledgment

This work was supported in part by the Research Grants Council of the Hong Kong Special Administrative Region,

China, under project 7131–12E, and by the NSFC RGC grant under project N–HKU714–13.

REFERENCES

1. T.-C. Poon, *Optical Scanning Holography with MATLAB* (Springer, 2007).
2. E. Y. Lam, X. Zhang, H. Vo, T. C. Poon, and G. Indebetouw, "Three-dimensional microscopy and sectional image reconstruction using optical scanning holography," Appl. Opt. **48**, H113–H119 (2009).
3. J.-P. Liu, "Spatial coherence analysis for optical scanning holography," Appl. Opt. **54**, A59–A66 (2015).
4. P. W. M. Tsang, J.-P. Liu, and T.-C. Poon, "Compressive optical scanning holography," Optica **2**, 476–483 (2015).
5. H. Ou, H. Pan, E. Y. Lam, and B.-Z. Wang, "Defocus noise suppression with combined frame difference and connected component methods in optical scanning holography," Opt. Lett. **40**, 4146–4149 (2015).
6. L.-Z. Zhang, J.-P. Hu, D.-M. Wan, X. Zeng, C. M. Li, and X. Zhou, "Innovative measurement of parallelism for parallel transparent plate based on optical scanning holography by using a random-phase pupil," Appl. Opt. **54**, 2483–2488 (2015).
7. E. Y. Lam, "Computational sectioning and resolution enhancement in optical scanning holography," in *OSA Topical Meeting in Digital Holography and Three-Dimensional Imaging* (Optical Society of America, 2014), paper DTu2B.1.
8. G. Indebetouw, Y. Tada, J. Rosen, and G. Brooker, "Scanning holographic microscopy with resolution exceeding the Rayleigh limit of the objective by superposition of off-axis holograms," Appl. Opt. **46**, 993–1000 (2007).
9. J. Ke, T.-C. Poon, and E. Y. Lam, "Depth resolution enhancement in optical scanning holography with a dual-wavelength laser source," Appl. Opt. **50**, H285–H296 (2011).
10. H. Ou, T.-C. Poon, K. K. Y. Wong, and E. Y. Lam, "Depth resolution enhancement in double-detection optical scanning holography," Appl. Opt. **52**, 3079–3087 (2013).
11. H. Ou, T.-C. Poon, K. K. Y. Wong, and E. Y. Lam, "Enhanced depth resolution in optical scanning holography using a configurable pupil," Photon. Res. **2**, 64–70 (2014).
12. G. Indebetouw, A. E. Maghnouji, and R. Foster, "Scanning holographic microscopy with transverse resolution exceeding the Rayleigh limit and extended depth of focus," J. Opt. Soc. Am. A **22**, 892–898 (2005).
13. G. Indebetouw, W. Zhong, and D. Chamberlin-Long, "Point-spread function synthesis in scanning holographic microscopy," J. Opt. Soc. Am. A **23**, 1708–1717 (2006).
14. T.-C. Poon and K. B. Doh, "On the theory of optical Hilbert transform for incoherent objects," Opt. Express **15**, 3006–3011 (2007).
15. D. P. Ghai, P. Senthilkumaran, and R. Sirohi, "Single-slit diffraction of an optical beam with phase singularity," Opt. Lasers Eng. **47**, 123–126 (2009).
16. J. M. Hickmann, E. J. S. Fonseca, W. C. Soares, and S. Chvez-Cerda, "Unveiling a truncated optical lattice associated with a triangular aperture using lights orbital angular momentum," Phys. Rev. Lett. **105**, 053904 (2010).
17. A. Ambuj, R. Vyas, and S. Singh, "Diffraction of orbital angular momentum carrying optical beams by a circular aperture," Opt. Lett. **39**, 5475–5478 (2014).
18. Y. Pan, W. Jia, J. Yu, K. Dobson, C. Zhou, Y. Wang, and T.-C. Poon, "Edge extraction using a time-varying vortex beam in incoherent digital holography," Opt. Lett. **39**, 4176–4179 (2014).
19. N. Chen, Z. Ren, A. Chan, X. Sun, and E. Y. Lam, "Depth enhancement of optical scanning holography with a spiral phase plate," in *OSA Topical Meeting in Digital Holography and Three-Dimensional Imaging* (Optical Society of America, 2015), paper DW2A.3.
20. J. A. Davis, D. E. McNamara, D. M. Cottrell, and J. Campos, "Image processing with the radial Hilbert transform: theory and experiments," Opt. Lett. **25**, 99–101 (2000).
21. C.-S. Guo, Y.-J. Han, J.-B. Xu, and J. Ding, "Radial Hilbert transform with Laguerre Gaussian spatial filters," Opt. Lett. **31**, 1394–1396 (2006).
22. G. Indebetouw, P. Klysubun, T. Kim, and T.-C. Poon, "Imaging properties of scanning holographic microscopy," J. Opt. Soc. Am. A **17**, 380–390 (2000).
23. X. Zhang, E. Y. Lam, and T.-C. Poon, "Reconstruction of sectional images in holography using inverse imaging," Opt. Express **16**, 17215–17226 (2008).